Korean J. Chem. Eng., 40(1), 124-135 (2023)
DOI: 10.1007/s11814-022-1203-3

pISSN: 0256-1115
eISSN: 1975-7220

Magnetic sodium alginate/hydroxyapatite nanocomposite as an efficient biosorbent for rapid adsorption of methylene blue

Mahboubeh Jourbonyan*, Mehrnaz Safarnia, Foad Raji***, and Ahmad Dadvand Koohi*,†**

*Chemical Engineering Department, Engineering Faculty, University of Guilan, Rasht, Iran
**Department of Chemical Engineering, Faculty of Engineering, Ferdowsi University of Mashhad, 91779489746
***School of Chemical Engineering, University of Queensland, Brisbane, Queensland 4072, Australia
(*Received 11 March 2022 • Revised 29 May 2022 • Accepted 10 June 2022*)

Abstract−The current study highlights the synthesis of a novel biosorbent for methylene blue (MB) removal from aqueous solutions. The biosorbent was synthesized by modifying sodium alginate biopolymer (SA) with hydroxyapatite (HAp) and Fe_3O_4 magnetic nanoparticles (M). The surface morphology was analyzed with SEM images. XRD and BET investigated the solid's structures, functional groups were identified by FTIR spectroscopy, and the magnetization behavior of the prepared adsorbents was investigated using VSM. The uptake of MB was investigated with respect to pH, initial dye concentration, sorbent dosage, and contact time. Studying the sorption kinetics revealed that diffusion of MB cations from the solution bulk to the solids' surface was the rate-limiting step of the sorption. The results showed that the biosorption of methylene blue is mainly a physical process. Based on Langmuir isotherm, the maximum capacity of the SA-HAp, SA-M, and SA-M-HAp was obtained as 511.3, 538.3, and 588.2 mg/g at 25 °C, respectively. Thermodynamic studies indicate that the adsorption process was exothermic and spontaneous. The SA-M-HAp biosorbent can be regenerated up to four cycles without significant reduction (less than 5%) in the sorption efficiency toward methylene blue. This study suggests that the SA-M-HAp composite is an excellent environmentally friendly adsorbent for removing cationic dyes from aqueous solutions.

Keywords: Adsorption Kinetics, Wastewater Treatment, Dye Removal, Magnetic Nanoparticles, Adsorption Mechanism

INTRODUCTION

The rapid growth of industrialization and human activity seriously threatens the natural environment. One of the most significant environmental concerns is the discharge of industrial dye effluent into surface and groundwater [1]. Synthetic dyes can cause serious health problems for humans, aquatic organisms, plants, and animals [1-3]. Therefore, removing synthetic dyes from wastewater streams before discharging them into the environment is essential. Methylene blue ($C_{16}H_{18}C_lN_3S$) is a common cationic dye with wide application in various industries, such as textiles, paper, leather, pharmaceuticals, food, and cosmetics. Various physicochemical and biological methods, such as ion exchange, flocculation, membrane separation, and adsorption, are used to eliminate dyes from wastewater [6-9]. Dye removal by adsorption is one of the most effective and preferred techniques as it is simple, highly efficient, and low-cost [10-12]. Another advantage is that various economical materials, such as natural zeolites, agricultural by-products, biomass, and industrial solid wastes, can be used as adsorbents [1,13,14].

Consistent with environmental protocols, eco-friendly, bio-degradable, and naturally abundant biopolymers have been used as green and renewable sorbents for pollutant removal from wastewaters [10,15-20]. Among the biopolymers, sodium alginate (SA) is a non-poisonous, low price, biodegradable, and highly efficient compound for removing aqueous contaminants [12,21]. Due to the presence of hydroxyl (-OH) and carboxylic (-COOH) functional groups, SA is highly hydrophilic, its surface can be easily modified, and the surface charge can conveniently be controlled by changing the solution pH [21,22]. However, the fragile nature (low thermal, chemical, and mechanical stability) and water-soluble properties of SA considerably influence its sorption performance. A proposed option to overcome this shortcoming is the ionic cross-linking process of SA adsorbent by substitution of sodium with divalent metal ions such as Ca^{2+}, Sr^{2+}, and Ba^{2+} [23]. Calcium chloride ($CaCl_2$) is known as the most common ionic cross-linker that can bind exclusively to the acidic structure of alginate (α-L-guluronic acid blocks) and improve the SA gelation [8]. Nanoparticles such as clays, silica, carbon nanotubes, iron oxide, graphene oxide, and hydroxyapatite as additives have been incorporated into the hydrogel structure to improve the stability of SA biopolymer [5,10,11,14,24,25]. Alamin and co-workers reported significant improvement in the MB sorption of SA after surface modification with activated carbon [26]. Alver et al. [2], using rice husk and magnetic nanoparticles, modified the structural properties of SA and obtained a maximum adsorption capacity of 274.9 mg/g for MB removal from aqueous solutions. The multi-walled carbon nanotube is another additive that has been used to improve the stability and sorption performance of SA hydrogel [10].

Hydroxyapatite (HAp), a green, bioactive, biodegradable substrate, has shown remarkable performance in the adsorption of heavy metal ions [13,17] and synthetic dyes [3,25,27] from aqueous solutions. HAp ($Ca_{10}(PO_4)_6(OH)_2$) can be extracted from mammalian bone (e.g., horse), aquatic sources (e.g., fishbone and fish scale), and

†To whom correspondence should be addressed.
E-mail: dadvand@guilan.ac.ir

minerals (e.g., limestone) [1,3,28]. Fish scales account for roughly 4% of the 18-31 million tons of dead fish waste discarded annually [13]. In this regard, fish scales can be considered a low-cost and naturally abundant source for HAp extraction. Due to phosphate (PO_4^{3-}) functional groups on the HAp surface, it has wide applications in the medical and pharmaceutical industries [29]. Moreover, HAp has shown exceptional ion exchange and sorption capacity for removing cationic pollutants from wastewater [3,17,30]. Therefore, the sodium alginate-hydroxyapatite (SA-HAp) nanocomposite can be considered an outstanding candidate for the sorption of cationic methylene blue from aqueous solutions. Further modification of SA-HAp with magnetic iron oxide (Fe_3O_4) nanoparticles can improve the surface area and stability of nanocomposite and can also make feasible the separation and reusability of solid particles after the sorption process using an external magnetic field [2,13, 14,23].

This study prepared a nanocomposite adsorbent by modifying alginate beads with HAp and Fe_3O_4 nanoparticles to evaluate its capability as an adsorbent for MB separation. Optimal experimental conditions were determined in terms of bulk pH, sorbent dosage, contact time, and MB concentration. The experimental results were fitted by different isotherm and kinetics models to determine the adsorption capacity, rate-limiting kinetics step, and sorption mechanism. The stability and reusability of the synthesized biosorbent were evaluated by tracing the MB sorption performance of the sorbent after several cycles of regeneration.

MATERIALS AND METHODS

1. Materials

Caspian kutum fish scales were obtained from a local market in Guilan, Iran. Methylene blue (MW=319.85 g/mol), ammonium hydroxide (NH_4OH), hydrochloric acid (HCl), calcium chloride ($CaCl_2$), and sodium hydroxide (NaOH) were purchased from Merck. Sodium alginate was a product of Sigma-Aldrich; $FeSO_4{\cdot}7H_2O$ and $FeCl_3{\cdot}6H_2O$ were obtained from Ghataran Shimi supplier in Iran. All the chemicals were used as received without further purification. All the aqueous solutions were prepared in deionized water.

2. Biosorbent Preparation

To synthesize HAp from fish scales, the fish scales were rinsed and cleaned with deionized water several times to remove contaminations and soluble dirt and dried in an oven at 90 °C for 48 h. The dried scales were washed with a copious amount of 0.1 M HCl (~1,000 mL) to remove the unwanted proteins. Eradication of the surface proteins was continued by stirring fish scales (600 rpm) in 400 mL of NaOH (2.5 M) for 1 h at 100 °C. Then, the white precipitates (HAp nanoparticles) were rinsed with deionized water and dried at 60 °C overnight. To prepare magnetic hydroxyapatite (M-HAp) nanoparticles, 4 g of $FeSO_4{\cdot}7H_2O$ and 7.76 g of $FeCl_3{\cdot}6H_2O$ (the molar ratio of Fe^{3+}/Fe^{2+}=2) [31] were dissolved in 100 mL deionized water and mixed for 20 minutes at 80 °C, then 1 g HAp was gradually added to the solution. pH was adjusted at 11 using ammonium hydroxide (25 wt% in water), and the solution temperature increased to 80 °C. The observed alteration in the solution color from pale yellow to dark brown indicated the formation of M-HAp nanoparticles. After filtering the obtained product, it was rinsed with deionized water to remove the unreacted chemicals and reach a neutral pH and was dried in an oven at 80 °C overnight.

To synthesize magnetic sodium alginate (SA-M), 2% w/v of sodium alginate in deionized water was mixed on a magnetic stirrer for 2 h at room temperature. 0.5 g iron oxide nanoparticles were dispersed in water for 10 min ultrasonically and then gradually added to the sodium alginate solution. After 10 min stirring, the dispersed solution was added dropwise into 0.1 M $CaCl_2$ solution as the cross-linking agent. Calcium ion (Ca^{2+}) can improve the gelation of sodium alginate and form an ordered structure. The final product was filtered after 24 h, rinsed with deionized water, and stored in water at room temperature.

Magnetic sodium alginate-hydroxyapatite (SA-M-HAp) nanocomposite was prepared by dispersing 2% w/v of SA in deionized water on a magnetic stirrer for 2 h at room temperature. Then 1 g of M-HAp nanoparticles was gradually added to the mixture. After 10 min mixing, the solution was gradually added dropwise into 0.1 M $CaCl_2$ and reacted for 24 h. Finally, the solid product was filtered, rinsed with deionized water, and stored in water at room temperature.

The synthesis procedure of sodium alginate-hydroxyapatite (SA-HAp) was similar to SA-M-HAp preparation, but instead of M-HAp, 1 g HAp was added to the SA solution. Fig. 1 depicts the final products of the synthesized sorbents.

3. Batch Sorption Studies

A batch sorption experiment was conducted by adding specific amounts of the synthesized nanocomposites (0.01 to 0.3 g) to 50 mL of MB solution under different experimental conditions. The pH of the solutions was adjusted using standard solutions of HCl and NaOH (0.01-0.1 M) in the range of 2 to 12. The effects of various operating parameters, including bulk pH (from 2-12), contact time (up to 180 min), MB initial concentration (2-680 mg/L), and sorbent dosage (0.2-6 g/L), were investigated on the MB sorp-

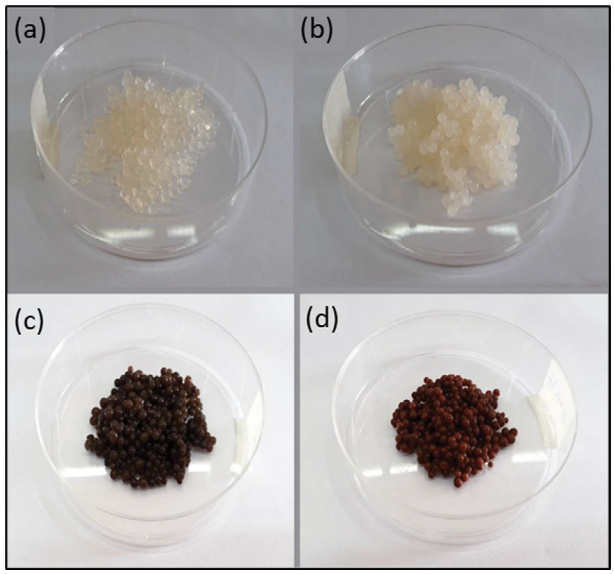

Fig. 1. Photographic pictures of (a) SA, (b) SA-HAp, (c) SA-M, and (d) SA-M-HAp.

tion efficiency (% removal) and adsorption capacity (mg/g) of the synthesized sorbents. The thermodynamic properties, including the sorption enthalpy (ΔH^0), entropy (ΔS^0), Gibbs free energy (ΔG^0) were analyzed by measuring the MB sorption capacity of the biosorbents with varying the solution temperature from 25 to 45 °C (pH 11, C_0 of MB=2-680 mg/L, and 1 g/L sorbent dosage). To study the effect of each parameter, other parameters were kept constant. The kinetics of the MB sorption was analyzed using pseudo-first-order, pseudo-second-order, film diffuson, and intraparticle diffusion models. Moreover, the sorption behavior and maximum MB sorption capacity of the sorbents were studied by Langmuir, Freundlich, and Dubinin-Radushkevich (DR) isotherms. The stability and reusability of the biosorbents were tested through the acid-wash technique. After MB sorption, the reacted biosorbent was separated from the solution, washed with deionized water, and mixed for 30 min in 300 mL of 0.1 M HCl at room temperature. Then, the solid beads were removed from the acidic solution, washed with deionized water, and used in the next sorption cycle without any surface modification.

For each sorption experiment, the concentration of MB in the supernatant was measured using UV spectrophotometers (Cary 50 bio UV-visible) by monitoring changes at a wavelength of maximum absorbance (664 nm). Eqs. (1) and (2) have been used, respectively, for determining the amount of MB sorption (mg/g) and removal efficiency (%) from aqueous solutions [32]:

$$q_e = \frac{(C_0 - C)V}{m} \quad (1)$$

$$\%R = \frac{(C_0 - C)}{C_0} \times 100 \quad (2)$$

where q_e (mg/g), C_0 (mg/L), and C (mg/L) are the sorption capacity, initial and equilibrium MB concentrations, respectively. V (L) is the solution volume, and m (g) refers to adsorbent dosage.

4. Characterization

Fourier transform infrared (FT-IR) spectroscopy (Nicolet 560, USA) was used for collecting the IR spectra of the synthesized materials in the frequency region of 400-4,000 cm^{-1} by a standard KBr technique. A Philips Analytical X-ray (XRD) BV diffractometer equipped with a Cu-anode measured the powder diffraction patterns in the 2θ range of 10° to 70° at 0.03° steps and 0.4 [s] scan step time. Scanning electron microscopy (FESEM, TESCAN MIRA3, Czech Republic) was used to analyze the structural morphologies of the solid beads and investigate elemental composition changes after methylene blue sorption using energy-dispersive X-ray spectroscopy (EDX) analysis. We analyzed the adsorption/desorption isotherms and porosity using BET (BELSORP MINI II. Microtrac Bel Corp, Japan) to determine the overall surface area and pore size distribution. Magnetization measurements for Fe_3O_4, SA-M, and SA-M-HAp were obtained using a vibrating sample magnetometer (LBKFB model, Meghnatis Kavir Kashan, Iran).

RESULTS AND DISCUSSION

1. FTIR and XRD Studies

Fig. 2 displays the FTIR spectra of the synthesized sorbents (SA,

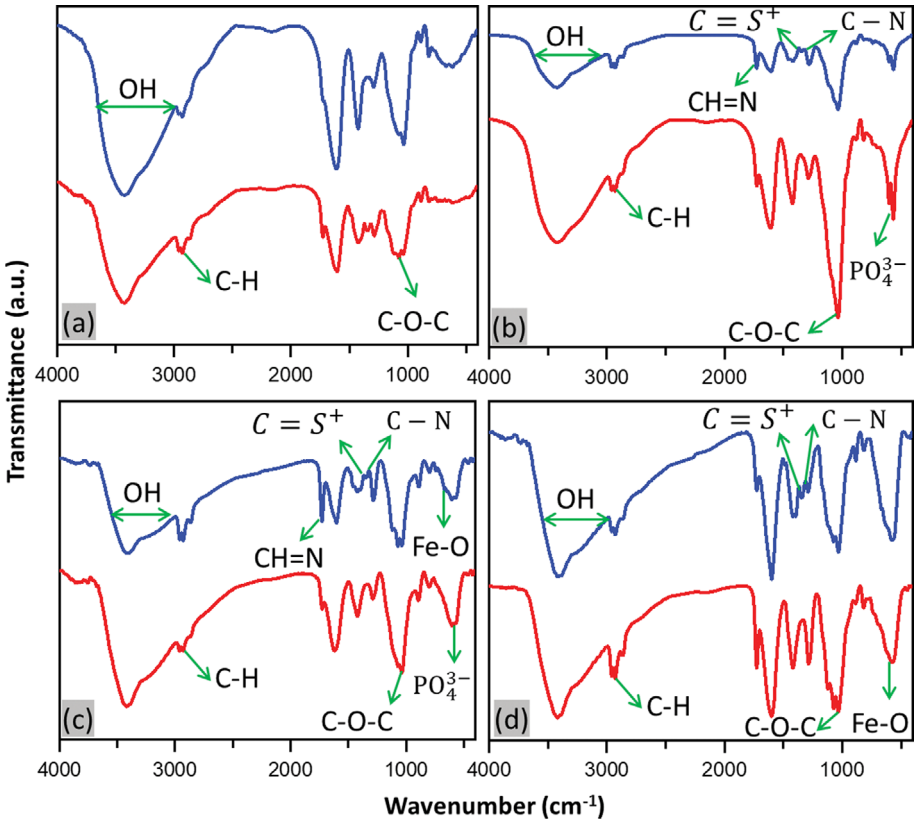

Fig. 2. FTIR spectra of (a) SA, (b) SA-HAp, (c) SA-M-HAp, and (d) SA-M sorbents before (red) and after methylene blue sorption (blue).

SA-HAp, SA-M, SA-M-HAp) before and after MB sorption. In summary, the significant and characteristic vibrational bands for all the prepared samples are (1) 578 cm^{-1} for the Fe-O group, (2) 3,000-3,600 cm^{-1} for surface hydroxyl (-OH) groups, (3) ~2,930 cm^{-1} indicates symmetric stretch vibration of $-CH_2$ and $-CH_3$ groups. For SA, the peak at 1,034 cm^{-1} describes the stretching vibration of cyclic ether (C-O-C), and the observed absorption bands between 1,540-1,700 cm^{-1} are related to the stretching vibrations of $-COO^-$ surface groups [22]. The peak at 819 cm^{-1} is attributed to the Na-O [33]. For HAp, the indicative phosphate peaks can be observed at 566 and 1,070 cm^{-1} [34] Also, the vibrational bands around 600 and 340 cm^{-1} are attributed to the HAp hydroxyl groups [27]. According to the reported vibrational frequencies of methylene blue [35], the peak at 1,626 cm^{-1} is attributed to the C=N and C=C, and 1,300-1,350 cm^{-1} can be attributed to the C-N (dimethylamino) and the $C=S^+$ vibrations of methylene blue. Alterations in the intensity of these peaks indicate this cationic dye's sorption on the surface of prepared sorbents. For SA-HAp and SA-M-HAp, the observed shifts in the position of PO_4^{3-} absorption bands imply the direct interaction of methylene blue with phosphate groups. Similarly, the alterations in the frequency and intensity of $-COO^-$ peaks reveal the role of this functional group on the sorption of methylene blue. Although some change in the intensity and frequency of some bands was observed after the sorption of methylene blue, these alterations were weak, which implies that the sorption of MB on the surface of the biosorbents mainly occurred through physical forces.

The XRD patterns of the synthesized samples are shown in Fig. 3. New characteristic peaks in the XRD pattern of M-SA approve the presence of Fe_3O_4 nanoparticles on the SA surface. The peaks at 2θ=26° and 32° are assigned to the crystalline structure of HAp,

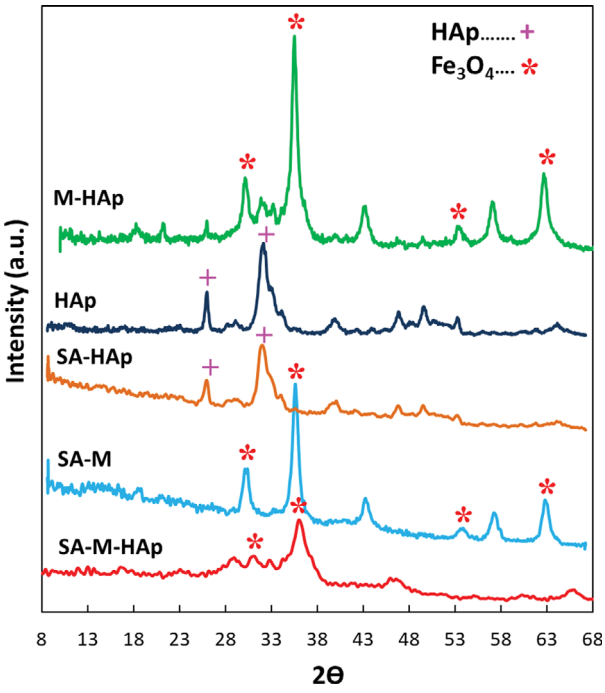

Fig. 3. X-ray diffraction patterns of M-HAp, HAp, SA-HAp, SA-M, and SA-M-HAp.

Table 1. Physico-chemical properties of the alginate-based adsorbents

Samples	S_{BET} (m^2g)	V_{BJH} [c^3(STP)/g]	d_{avg} (nm)
SA-HAp	7.9	0.027	13.81
SA-M	15.2	0.061	15.92
SA-M-HAp	28.6	0.158	22.04

while the distinctive peaks of crystalline Fe_3O_4 and semi-crystalline SA biopolymer can be found at 2θ=30°, 35°, 54°, and 63° and 2θ=13°, and 21°, respectively [29,36]. For composites containing SA biopolymer, the observed broad diffraction peaks at 2θ less than 20° indicates the presence of amorphous alginate [14]. For SA-M-HAp, the intensity of Fe_3O_4 characteristic peaks has considerably decreased due to the presence of HAp particles. The obtained XRD patterns confirm the successful loading of HAp and Fe_3O_4 particles into the SA hydrogel network.

2. BET and Vibrating-sample Magnetometry (VSM) Analysis

The results of Brunauer-Emmett-Teller (BET) surface area of SA-HAp, SA-M, and SA-M-HAp adsorbents are listed in Table 1. Large pore volumes and specific surface areas may explain the high adsorption capacity of the adsorbents. The results show that incorporating Fe_3O_4 and HAp nanoparticles into the SA matrix has improved the surface area of the adsorbent. The vibrating-sample magnetometry (VSM) analysis (Fig. 4) was carried out to investigate the magnetic properties of the synthesized Fe_3O_4, SA-M, and SA-M-HAp composites at room temperature. The saturation magnetization of 57.4 emu/g and lack of hysteresis loop and coercivity confirmed the superparamagnetic behavior of the synthesized magnetic iron oxide nanoparticles [37]. The synthesized SA-M and SA-M-HAp showed saturation magnetization values in the order of 26 and 16.6 emu/g, respectively, which are evidently less than the obtained value for pure Fe_3O_4. The higher reduction of saturation magnetization for SA-M-HAp than SA-M can be related to the lower content of Fe_3O_4 particles in bulk or on the surface SA-M-HAp, size of the particles, composite coating, and the isolation effect of SA and HAp. However, almost no hysteresis loop was found in the magnetization curves of SA-M and SA-M-HAp, suggesting the

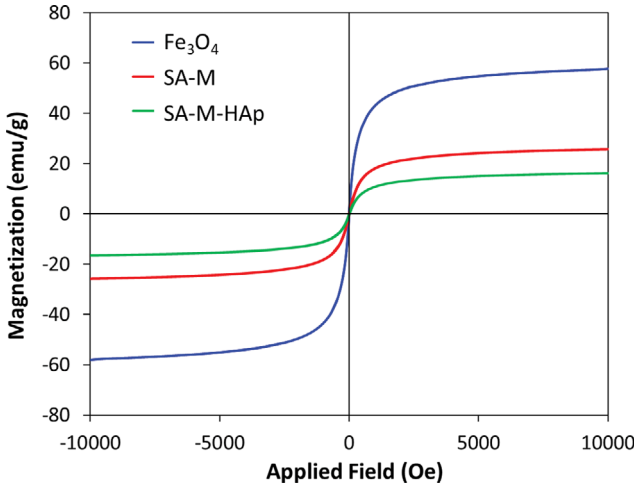

Fig. 4. Magnetization curve of adsorbents at room temperature.

superparamagnetic feature of these particles and their ability to be separated from aqueous solutions several times without losing their magnetic character. The superparamagnetic feature of these particles reveals the lack of magnetic agglomeration of the particles after removing the magnetic field from the medium [38].

3. Adsorbents Morphology

Fig. 5 exhibits the SEM micrographs of SA, SA-HAp, SA-M, and SA-M-HAp adsorbents before and after MB sorption. Fig. 5(a) demonstrates that the SA adsorbent has a smooth and homogeneous surface, while MB has uniformly covered the SA surface after adsorption and changed its chemistry. After adding hydroxyapatite nanoparticles to the alginate, surface heterogeneity increased, as revealed in the surface morphology of the SA-HAp adsorbent (Fig. 5(b)). Similar alterations in the surface morphology of SA-M are clear in Fig. 5(c). The adsorbent had a homogeneous surface before magnetization but became heterogeneous after modifying with magnetic nanoparticles. The nanoparticles are visible on the adsorbent surface, indicating that Fe_3O_4 particles have been successfully loaded on the surface. It was observed that the alginate biopolymer covers the Fe_3O_4 nanoparticles, which protects these nanoparticles from oxidation [29]. The diameters of some Fe_3O_4 nanoparticles loaded on the adsorbent are shown in SEM images with an average diameter of around 30 nm (Fig. 5(c)). As shown in Fig. 5(d) for the SA-M-HAp biosorbent, after modification of the SA with M-HAp nanoparticles, the surface of the adsorbent has changed, and nanoparticles are visible on the adsorbent surface. It can be seen in Fig. 5(d) that magnetite nanoparticles envelop hydroxyapatite. As a result of its spherical geometry and porous structure, dye molecules could easily be sorbed on the surface [39].

EDX analysis (Table 2) provided further evidence for the sorption of MB on the surface of synthesized nanocomposites. SA solution was added to calcium chloride to produce an amorphous structure, and the EDX results reveal that some of the Ca and Cl ions remained in the structure of the prepared sorbents. The apearance of Fe and P elements implies the presence of Fe_3O_4 and HAp on the prepared samples, respectively. In agreement with FTIR and XRD data, EDX results confirmed the successful modification of SA with magnetic Fe_3O_4 and HAp nanoparticles. Regarding the

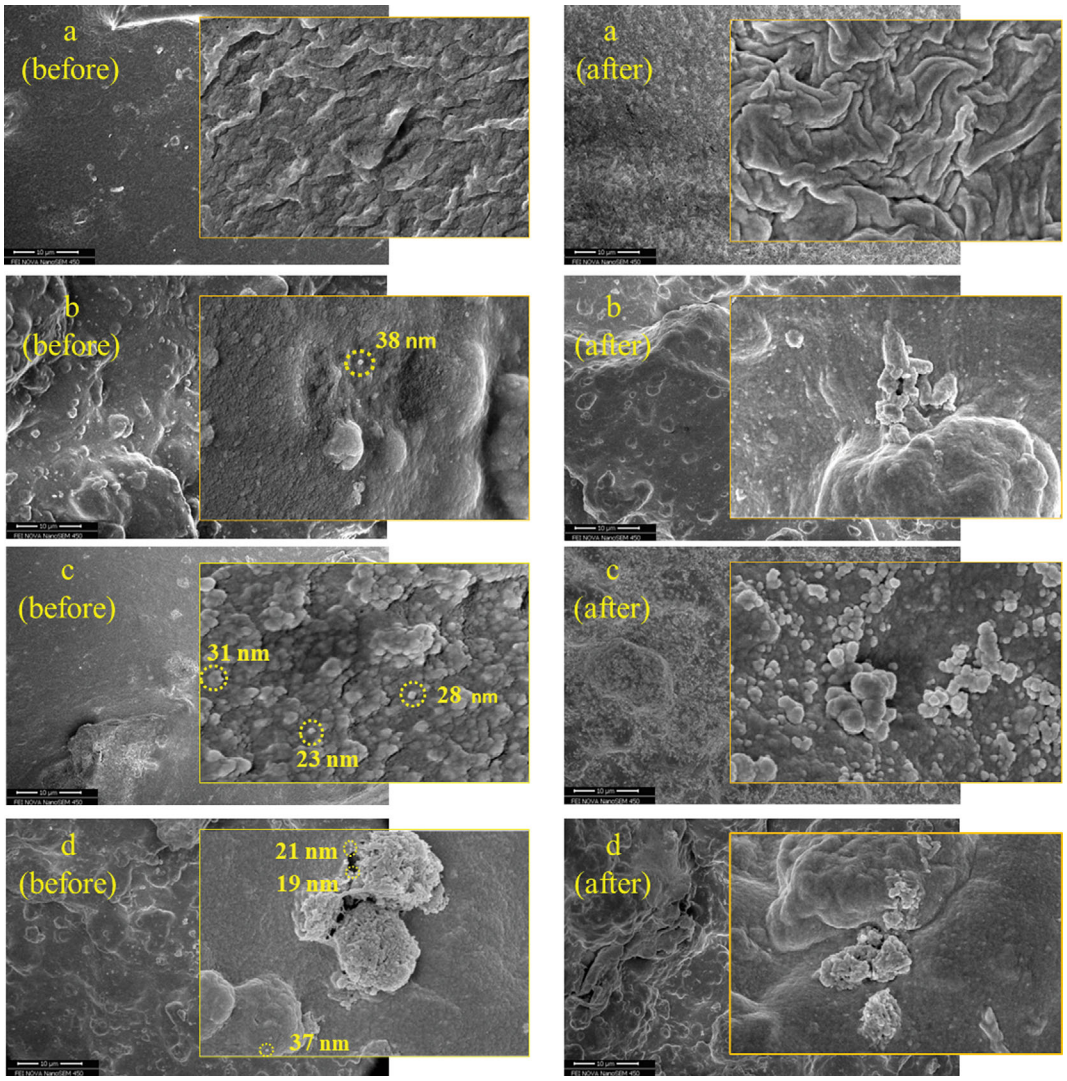

Fig. 5. SEM images of (a) SA, (b) SA-HAp, (c) SA-M, and (d) SA-M-HAp before and after methylene blue sorption.

Table 2. EDX data of (a) SA, (b) SA-M, **(c)** SA-HAp, and (d) SA-M-HAp before and after methylene blue sorption

Sorbent \ Element (wt%)		O	C	Ca	P	N	S	Cl	Na	Fe
SA	Before	52.11	32.83	10.65	-	-	-	0.27	0.16	-
	After	38.30	46.54	4.14	-	3.17	0.42	0.46	0.50	-
SA-M	Before	50.96	41.13	6.33	-	-	-	0.32	0.13	4.90
	After	38.41	45.37	5.19	-	4.33	0.89	0.09	0.88	3.09
SA-HAp	Before	46.33	41.67	4.42	0.96	-	-	0.36	0.31	-
	After	40.04	45.43	3.55	1.64	3.65	0.52	0.28	1.51	-
SA-M-HAp	Before	47.74	39.58	5.74	1.89	-	-	0.14	0.35	8.64
	After	42.47	42.77	2.99	0.91	5.14	1.31	0.13	0.77	4.64

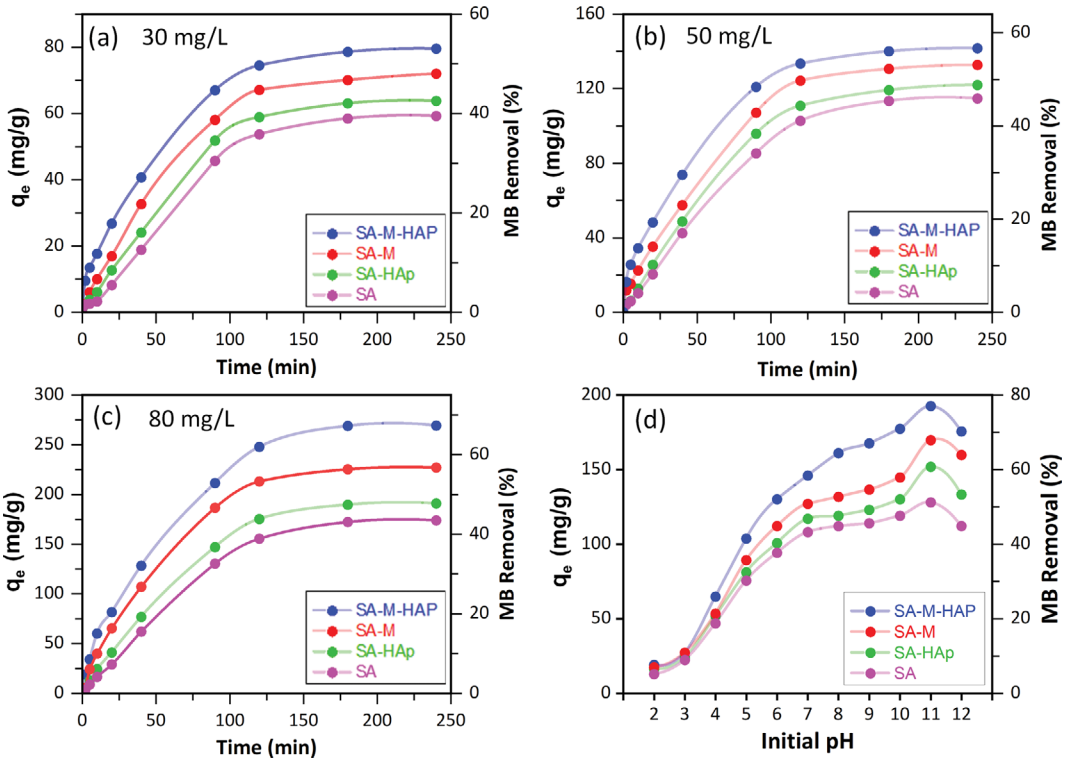

Fig. 6. The effect of contact time on the adsorption capacity of methylene blue onto SA, SA-M, SA-HAp, and SA-M-HAp biosorbents at (a) 30, (b) 50, and (c) 80 mg/L initial concentration of methylene blue (at 25 °C, pH 7, and 0.2 g/L sorbent dosage). (d) effect of pH on the sorption capacity of methylene blue by biosorbents (at 25 °C, 50 mg/L methylene blue, and 1 g/L sorbent dosage).

main elements in the structure of methylene blue (C, N, S, Cl, H), detection of nitrogen (N) and sulfur (S) on the surface of examined sorbents indicated the MB sorption.

4. Effect of Contact Time and Initial pH

Fig. 6 illustrates the effect of contact time on the sorption capacity (mg/g) of biosorbents for solutions containing 30, 50, and 80 mg/L of MB. The sorption of MB increased with time and reached its equilibrium amount after 180 min. Independent of initial MB concentration, the equilibrium time was approximately similar for all the investigated sorbents. For all the sorbents, the initial sorption rate was very fast within the first 90 min of the sorption process and then gradually decreased and reached equilibrium. This rapid sorption can be associated with the high free energy of active surface sites toward the cationic MB species, increasing the concentration gradient between solution bulk and surface functional groups [26]. Increasing the time will increase the saturation of active surface sites and reduce the number of vacant sites for further sorption of MB. Also, electrostatic repulsion between the sorbed MB species and MB cations in the liquid phase can reduce the rate of sorption efficiency. Higher initial concentrations lead to more penetration of MB from solution bulk into the electric double layer at the interface of liquid solution-charged sorbent due to the high driving force in concentrated solutions, which eventually results in higher MB sorption efficiency and capacity [26,40]. The maximum amount of adsorbed MB by the SA-M-HAp adsorbent increased from 80 to 270 mg/g when the MB concentration rose from

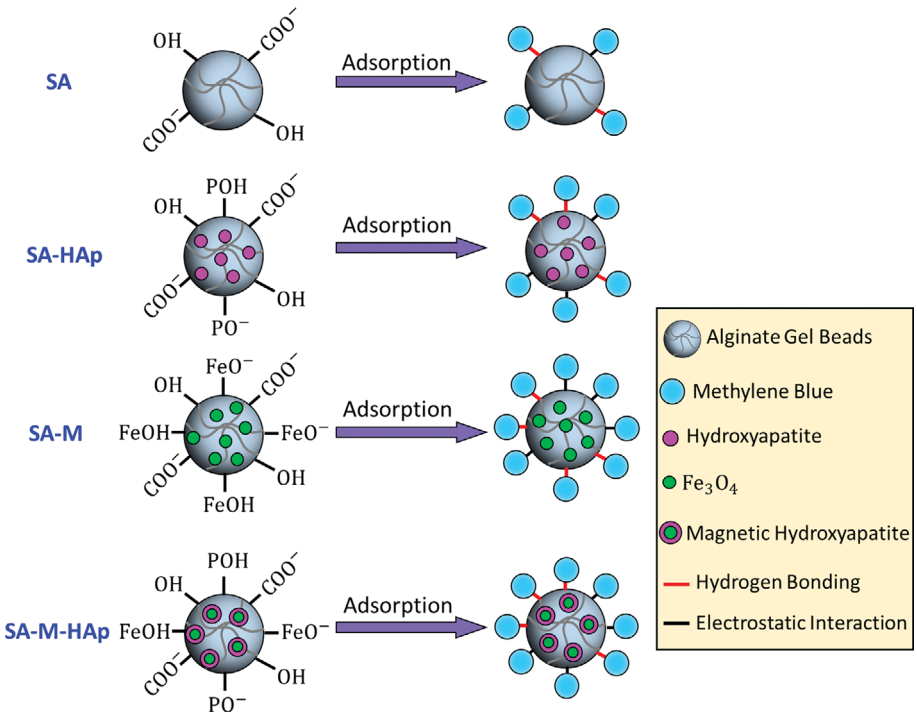

Fig. 7. Schematic representation for the methylene blue sorption mechanisms by the synthesized biosorbents.

30 to 80 mg/L.

The initial pH of solutions is one of the most significant factors that affect the ionization degree and molecular structure of cationic MB and also the surface charge density of solid surfaces due to the protonation (at low pH) and deprotonation (at high pH) of surface functional groups (Fig. 6(d)). Because of the presence of hydroxyl (-OH) and carboxylic (-COOH) functional groups, sodium alginate is negatively charged at pH>2 [27], and the reported isoelectric points (IEPs) for magnetite (Fe_3O_4) and hydroxyapatite [41] are around pH 5 and 8, respectively, which show Fe_3O_4 and HAp carry negative charges at pH above their corresponding IEPs. Due to the low surface charge density at low pH<4 and also the competition between H^+ and cationic MB for occupying the available surface sites, the sorption capacity and removal efficiency of all the investigated sorbents were very low. For pH>5, the negativity of the surface charge increases for all the solid sorbents (regarding the IEP of the sorbents), and stronger electrostatic attraction between cationic MB and negative active sites leads to the increment of q_e and removal efficiency. Compared to SA, higher values of q_e were obtained for SA-HAp and SA-M at pHs above 7 and 5, respectively, which can be attributed to the IEPs of magnetite (IEP~5) and HAp (IEP~8) and stronger electrostatic attraction between MB and negative surface sites at pHs>IEP. For SA-M-HAp, the simultaneous presence of both Fe_3O_4 and HAp materials on the surface of SA increased the population of negatively charged surface sites ($-O^-$, $-COO^-$, $-Fe-O^-$, and $-PO_4^{3-}$) and, consequently, the higher driving force between these negatively charged sites and MB has enhanced q_e. The maximum sorption capacity was obtained at pH~11. For pH>11, the high concentration of Na^+ (1 mM) in the solution and their competition with cationic MB for the negative surface sites, the value of q_e reduced. The mechanism of MB adsorption by the synthesized adsorbents is shown in Fig. 7. Adsorption mainly occurs through electrostatic interactions between sodium alginate hydroxyl and carboxyl groups and MB cations. After incorporating HAp nanoparticles into the SA matrix, phosphate functional groups interacted with MB cations and improved the sorption efficiency [25].

5. Effect of Sorbent Dosage and Initial Dye Concentration

Fig. 8(a) illustrates the MB sorption capacity and removal efficiency as a function of the sorbent dosage at equilibrium conditions. With increasing sorbent dosage, the removal efficiency of MB increased because more surface area and binding sites were available for the sorption of cationic dye. However, the sorption capacity (q_e) of MB reduced with increasing the amount of sorbents in the solution ($q_e \propto 1/m$). Higher sorption capacity at a lower dosage is associated with exposure of binding sites to the excessive mass of MB cations, leading to the saturation of most surface sites and, finally, more adsorption capacity. On the other hand, at higher sorbent dosages, the population of unoccupied surface sites increases, which reduces the ratio of occupied to total surface sites and consequently decreases the magnitude of sorption capacity [32]. For SA-M-HAp, the adsorption capacity decreased from 180 to 5 mg/g when sorbent dosage increased from 0.2 to 6 g/L.

Fig. 8(b) illustrates the effect of the initial dye concentration (C_0= 2-680 mg/L) on the sorption capacity and removal efficiency of MB at 25 °C and pH 7. In contrast to the sorbent dosage, the sorption capacity has increased with increasing C_0. In contact with more MB cations, the possibility of interaction between MB and active surface sites increases and will lead to greater sorption of cationic dye by the biosorbents. Therefore, for a constant mass of sorbent (1 g/L), increasing the C_o leads to the saturation of surface sites and enhances the sorption capacity (q_e). On the other hand, in-

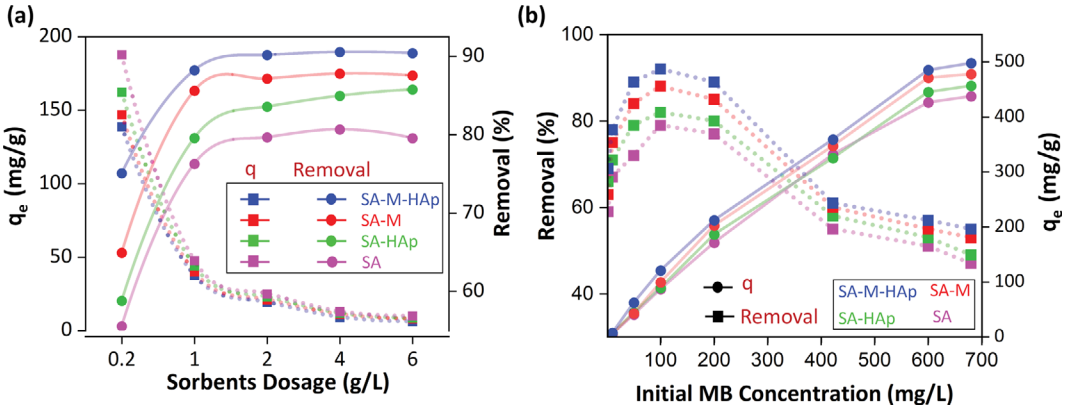

Fig. 8. The sorption capacity and removal efficiency of MB by the synthesized biosorbents as a function of (a) sorbent dosage (g/L) at 25 °C, pH 11, and C_0=50 mg/L, and (b) initial methylene blue concentration (mg/L) at 25 °C, pH 11, and sorbent dosage of 1 g/L.

creasing the MB concentration up to 100 mg/L increased the removal efficiency for all the biosorbents. Further increment in the C_0 leads to a considerable reduction in the removal efficiency. The initial increase of MB removal (%) probably can be due to the increase in the mass gradient (driving force) between the dye solution and the biosorbent surface. The removal efficiency declined at higher C_0>100 mg/L because (1) the number of vacant surface sites was reduced, and there was no free space for further sorption of MB cations, and (2) the accumulation of MB cations near the surface repelled the bulk cations.

6. Adsorption Kinetics and Isotherm Models

Kinetics of the sorption process was analyzed using reaction and diffusion models to gain valuable information regarding the reaction rate and the underlying MB sorption mechanism on the surface of biosorbents. For reaction models, such as pseudo-first-order and pseudo-second-order, the rate of sorption is determined following chemical reactions/complexations between the sorbate (A) and the solid surface (S),

$$A+S \rightleftharpoons AS;\ K_1,\ K_2 \tag{3}$$

where K_1 and K_2 are the rate constants for adsorption and desorption, respectively. The sorption reactions can proceed through physical and chemical forces between sorbate and the sorbent surface. Physical adsorption stems from the weak attraction like van der Waals forces between molecules and solid surface, while chemical adsorption involves the formation of a strong chemical force like covalent and ionic bonds. The pseudo-first-order and pseudo-second-order are the most common models for describing the chemical/physical sorption of pollutants from aqueous solutions.

The pseudo-first- and second-order models are expressed by Eqs. (4) and (5), respectively;

$$q_t = q_e(1-e^{-k_1 t}) \tag{4}$$

$$q_t = \frac{q_e^2 k_2 t}{1+k_2 q_e t} \tag{5}$$

where, q_t and q_e (mg/g) are the amount of sorbed methylene blue at t (min) and equilibrium, respectively. k_1 (min^{-1}) and k_2 (g/mg/min) are the rate constants of the pseudo-first- and second-order models, respectively.

In addition to the reaction-based model, the sorption kinetics can be described using the diffusion models. The diffusion of sorbate from bulk solution into the electrical double layer around the solid surface is called the boundary layer of film diffusion. For porous solids, sorbate can diffuse into the sorbent pores after film diffusion and interact with intraparticle surface sites. After the film and intraparticle diffusion, sorbate can rapidly be sorbed on the surface through physical or chemical interaction. Since the last step is very fast, one of the film or intraparticle diffusion should be the rate-limiting step for the sorption kinetics.

For spherical particles, the film diffusion model can be expressed as follows:

$$\ln\left(\frac{C_t}{C_0}\right)_{t\to 0} = -k_f \beta t \tag{6}$$

in which k_f represents the film mass transfer coefficient, C_t and C_0 are the concentration of methylene blue at time t and zero, and β is a constant that depends on the physical properties of the sorbent such as density, mass, radius, and volume.

The BET analysis revealed that the prepared sorbents are porous and have an average diameter above 15 nm (Table 1). Therefore, methylene blue molecules can penetrate the porous structure of the biosorbents and be captured through the intraparticle diffusion mechanism. The Weber and Morris equation (Eq. (7)) is a typical form of intraparticle diffusion where k_i is the intraparticle diffusion constant (mg/g/$min^{0.5}$), t is the reaction time, and I is a constant related to the extent of the boundary layer thickness.

$$q_t = k_i t^{0.5} + I \tag{7}$$

Table 3 presents the results of electrokinetics analysis for the sorption of methylene blue by bare (SA) and modified (SA-M-HAp) sodium alginate hydrogels using reaction-based and diffusion-based models. For the reaction models, the lowest correlation coefficient (R^2) was obtained for the pseudo-second-order model. The higher R^2 value for pseudo-first-order than pseudo-second-order model implies the physical sorption of MB on the surface of the synthesized biosorbents [28]. Regarding the pseudo-second-order model, the obtained R^2 values for SA-M-HAp are remarkably higher than

Table 3. Kinetics parameters for methylene blue adsorption by the alginate-based biosorbents

Kinetic models	Parameters	SA Dye concentration (mg/L)			SA-M-HAp Dye concentration (mg/L)		
		30	50	80	30	50	80
Pseudo-first order	q_e (mg/g)	66.42	127.74	195.25	73.32	136	213.17
	k (min^{-1})	0.020	0.019	0.018	0.022	0.022	0.021
	R^2	0.963	0.965	0.969	0.974	0.974	0.978
Pseudo-second order	q_e (mg/g)	108.69	303.03	666.66	166.66	294.11	454.54
	k (mg/g/min)	6.7×10^{-5}	1.3×10^{-5}	3.8×10^{-6}	1.1×10^{-4}	1.7×10^{-4}	6.2×10^{-5}
	R^2	0.766	0.618	0.534	0.947	0.942	0.935
Film diffusion	$k_f\beta$ (min^{-1})	0.0038	0.0042	0.0045	0.0056	0.0062	0.0078
	R^2	0.9817	0.9813	0.9938	0.9931	0.9986	0.9981
Intraparticle diffusion	k_i (mg/g/$min^{0.5}$)	5.573	10.881	16.628	6.349	11.866	18.431
	I (mg/g)	−9.792	−20.413	−32.424	−11.739	−21.076	−31.439
	R^2	0.975	0.983	0.984	0.988	0.989	0.988

SA, which implies the presence of chemical interactions at the solid interface after modifying the surface of SA with Fe_3O_4 and hydroxyapatite. However, as the FTIR data show, these chemical interactions are less pronounced than physical interactions. Compared to reaction models, film and intraparticle diffusion models correlate better with experimental data. The highest R^2 for film diffusion model shows that the penetration of methylene blue molecules from bulk solution into the electrical double layer region of sorbents is the rate-limiting step of the sorption process. Moreover, the high R^2 values for the intraparticle diffusion model indicate that a significant portion of methylene blue molecules has penetrated the porous structure of the biosorbents and interacted with surface sites and/or trapped in the mesopores [42,43].

Three isotherm models, Langmuir, Freundlich, and Dubinin-Radushkevich, were used to fit the experimental results. Isotherm analysis provides key information regarding the maximum adsorption capacity, sorption mechanism, and monolayer or multilayer type of adsorption [32]. The coefficient of determination parameter (R^2) was used to investigate the correlation between the experimental data and the predicted isotherm values.

The Langmuir model assumes the formation of a homogeneous surface through a single adsorption layer which is expressed by the following equation [32]:

$$q_e = \frac{q_m K_L C_e}{1 + K_L C_e} \tag{8}$$

where q_e is the amount of adsorbed solute per unit weight of adsorbent at equilibrium (mg/g), C_e is the equilibrium MB concentration in the bulk solution (mg/L), q_m is the maximum adsorption capacity (mg/g), and K_L is the constant related to the free energy of adsorption (L/mg). From the Langmuir isotherm, the dimensionless equilibrium parameter, R_L, can be defined as Eq. (9) to determine whether the sorption process is favorable ($0<R_L<1$), unfavorable ($R_L>1$), linear ($R_L=1$), or irreversible ($R_L=0$) [44,45].

$$R_L = \frac{1}{1 + K_L C_0} \tag{9}$$

where K_L is the Langmuir constant and C_0 is MB initial concen-

Table 4. Langmuir, Freundlich, and D-R isotherm constants for methylene blue adsorption on the alginate-based gel beads

Kinetic models	Parameters	SA	SA-HAp	SA-M	SA-M-HAp
		Temprature=25 °C			
Langmuir	q_m (mg/g)	486.3	511.3	538.2	588.2
	K_L (L/mg)	0.0189	0.0189	0.0213	0.0294
	R^2	0.9979	0.9897	0.9957	0.9958
	R_L	0.327	0.324	0.319	0.123
Freundlich	K_F (mg/g)	54.4	55.6	58.6	80.6
	n	2.56	2.62	2.43	2.78
	R^2	0.9869	0.9841	0.9888	0.9882
Dubinin-Radushkevich	q_{mDR}	454.6	446.5	496.1	499.7
	β (mol^2/J^2)	8.5×10^{-9}	9.1×10^{-9}	9.9×10^{-9}	8.1×10^{-9}
	E (kJ/mol)	7.6	7.4	7.1	7.8
	R^2	0.9794	0.9566	0.9346	0.9744

Table 5. Maximum adsorption capacities (mg/g) of different adsorbents containing sodium alginate for methylene blue removal from aqueous solutions

Adsorbents	Maximum adsorption capacity (mg/g)	Ref.
Hydroxyapatite-sodium alginate	142.8	[25]
Hydroxyapatite-sodium metasilicate	163.4	[28]
Calcium alginate/graphene	181.8	[46]
Apatite/attapulgite/alginate composite	244.6	[12]
Halloysite nanotubes alginate	250.1	[47]
Activated carbon-alginate	287.3	[48]
Sodium alginate–flax seed ash beads	333.3	[8]
Sodium alginate-MOF-Graphene oxide composite	490.7	[5]
Biopolymeric composite of sodium alginate	522.4	[21]
Calcium alginate/organobentonite beads	799.4	[11]
Maghemite/alginate/carbon nanotubes	905.5	[10]
SA-M	538.2	This study
SA-HAp	511.3	This study
SA-M-HAp	588.2	This study

tration. Table 4 shows that the value of R_L for all the studied biosorbents falls in the range of 0 to 1, which implies the favorable shape of Langmuir isotherm for describing the MB sorption.

The Freundlich isotherm is an appropriate model for multilayer sorption on a heterogeneous surface and, in nonlinear form, can be expressed as follows [44]:

$$q_e = K_F C_e^{1/n} \tag{10}$$

where C_e is the equilibrium concentration of dye (mg/L), q_e is the amount of dye adsorbed per unit mass of adsorbent (mg/g), K_F and 1/n are the model constants attributed to capacity and intensity of adsorption obtained by plotting $\ln q_e$ vs. $\ln C_e$.

Also, the experimental data were fitted to the Dubbinin-Radushkevich (D-R) model to identify whether the sorption process was physical or chemical. The nonlinear form of D-R is expressed as follows [40]:

$$q_e = q_{mDR} e^{-\beta\varepsilon^2} \tag{11}$$

In this model, q_e represents the amount of adsorbate per unit weight of sorbent (mol/g), q_{mDR} is the maximum sorption capacity (mol/g), and β (mol^2/J^2) is the activity coefficient and is a function of sorption mean free energy (E, kJ/mol) as follows:

$$\varepsilon = RT\ln\left(1+\frac{1}{C_e}\right) \tag{12}$$

$$E = 1/\sqrt{-2\beta} \tag{13}$$

where ε is the Polanyi potential [44]. For E<8 kJ/mol the sorption mechanism is physical while 8<E<16 kJ/mol suggests the chemical nature of the sorption process [40]. Table 4 lists the Langmuir, Freundlich, and D-R parameters as well as the related correlation coefficients (R^2). The higher R^2 value for Langmuir isotherm reveals the homogenous and monolayer sorption of MB on the surface of biosorbents. The D-R model predicted the experimental data with correlation coefficients higher than 0.93. The sorption energy (E) for all the biosorbents was less than 8 kJ/mol, which indicates the physisorption of MB cations on the surface of biosorbents is the dominant sorption mechanism.

Table 5 represents a comparative study concerning the maximum sorption capacity (q_m) of MB using the examined biosorbents in this study with the reported alginate-based adsorbents in the literature. As a low-cost and eco-friendly biosorbent, the maximum uptake capacity of SA-M-HAp is considerably higher (588.2 mg/g) than most alginate-based sorbents. Additionally, K_L demonstrated an increase in the adsorptive properties of SA-M-HAp when compared to the other adsorbents. This improvement is directly related to the presence of HAp and Fe_3O_4 nanoparticles introduced to the alginate structure.

7. Adsorption Thermodynamics

Temperature is a key parameter for determining the feasibility and spontaneity of the sorption of pollutants from aqueous solutions. Fig. 9 shows the exothermic nature of MB sorption on the surface of biosorbents as the sorption capacities have decreased with increasing temperature from 25 to 45 °C. Thermodynamic parameters of MB sorption by the biosorbents can be obtained as per Eqs. (14) and (15) by measuring the equilibrium constants ($K = q_e/C_e$) as a function of temperature. The Gibbs free energy change (ΔG^o) is the fundamental criterion of spontaneity. Thermodynamically, a sorption process is considered spontaneous when $\Delta G^o < 0$ [49].

$$\Delta G^o = -RT\ln K \tag{14}$$

$$\ln K = \left(\frac{\Delta S^o}{R}\right) - \left(\frac{\Delta H^o}{RT}\right) \tag{15}$$

Table 6 presents the obtained thermodynamic parameters for MB sorption. The negative value of ΔG^o at investigated temperatures indicates the spontaneous nature of MB uptake by the biosorbents. The standard enthalpy change (ΔH^o) is negative for all the examined biosorbents and reveals that the MB sorption is an exo-

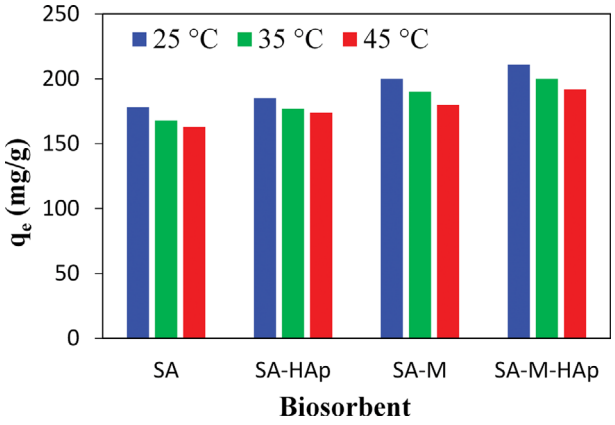

Fig. 9. Effect of temperature on the adsorption of MB onto SA, SA-Hap, SA-M, SA-M-HAp biosorbents (conditions: sorbent dosage=1 g/L; stirring speed=300 rpm; C_0=200 mg/L; pH 11).

Table 6. Thermal parameters for the methylene blue adsorption onto different adsorbents

Adsorbent	ΔH^o (kJ/mol)	ΔS^o (J/mol/K)	ΔG^o (kJ/mol)		
			25 °C	35 °C	45 °C
SA	−23.2	−63.5	−4.3	−3.6	−2.9
SA- HAp	−27.6	−76.2	−4.9	−4.1	−3.3
SA-M	−27.7	−74.1	−5.6	−4.8	−4.1
SA-M-HAp	−29.3	−76.5	−6.4	−5.9	−4.8

thermic process, and temperature rising will reduce the sorption capacity. The negative ΔS^o values imply that the sorbed MB cations on the surface of biosorbents are more ordered than the bulk solution [26,50]. Energetically, sorption due to the chemical forces (chemisorption) like covalent and ionic bonding is stronger than physical forces (physisorption) such as electrostatic and van der Waals interactions. In this regard, the heat of chemisorption varies from 80-200 kJ/mol, and physisorption falls in the range of 2.1-20.9 kJ/mol [49]. The obtained ΔH^o values in this study (Table 6) suggest that the uptake of MB by the biosorbents is a physisorption process.

8. Adsorbent Regeneration

Reusability and regeneration of the sorbents are significant factors for commercial applications to reduce the operational costs of wastewater treatment processes. Fig. 6(d) suggests that under acidic conditions (pH<4), the interaction of methylene blue with the surface of the biosorbents is very weak. Therefore, the acid-wash technique was employed for adsorbent regeneration. Fig. 10 shows a slight reduction in the sorption efficiency of methylene blue by SA-M-HAp from 88 to 84% after reusing for four cycles. The high reusability of SA-M-HAp implies the durability of the synthesized biosorbent and the physical sorption mechanism of methylene blue. At low pH, proton (H_3O^+) as a charge determining cation has a greater affinity toward the surface of biosorbent and interacts with surface hydroxyl groups much stronger than methylene blue. Therefore, under strongly acidic pH, (1) protonation of surface hydroxyls reduces the electrostatic attractions between cationic methylene

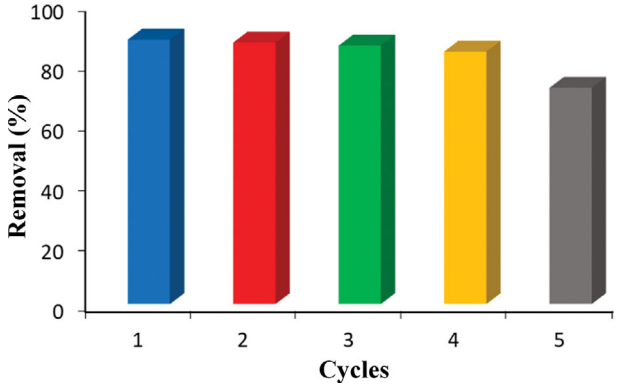

Fig. 10. Regeneration and reusability study of SA-M-HAp beads for five cycles using 0.1 M HCl.

blue and negative surface sites, and (2) cation exchange between physically sorbed methylene blue and protons leads to the diffusion of dye from surface sites to the bulk solution and facilitates the regeneration of SA-M-HAp biosorbent. For the fifth regeneration cycle, the sorption of methylene blue reduced from 84 to 72%. The higher reduction in the sorption of methylene blue might be due to alterations in the textural properties of the biosorbent like pore blocking and a decline in the number of active surface sites occupied by methylene blue. The regeneration tests revealed that the SA-M-HAp biosorbent is a cost-effective biosorbent that can be reused up to four cycles without considerably reducing the methylene blue uptake from aqueous solutions.

CONCLUSION

The ability of SA-M, SA-HAp, and SA-M-HAp to eliminate methylene blue dye from aqueous solution was studied in the current research. Certain parameters, such as contact time, pH, adsorbents concentration, and dye concentration, were studied to determine how they affect the methylene blue removal efficiency. The prepared SA-M-HAp adsorbent clarified the excellent MB adsorption capacity of 588.2 mg/g. FTIR spectra of adsorbents showed that COO^-, OH and PO_4^{3-} groups were involved in adsorption; however, weak alterations in the vibrational frequency of these functional groups suggest that physical interactions dominate the chemical forces. The SEM analysis showed a heterogeneous adsorbent after modifying the SA surface with magnetic Fe_3O_4 and hydroxyapatite nanoparticles, which changed to a smoother and less porous surface after dye adsorption. The kinetics of the process reveal that the film and intraparticle diffusion mechanisms are the main rate-limiting steps for the uptake of MB by the alginate based biosorbents. Thermodynamically, it was demonstrated that the MB sorption by the biosorbents was favorable, spontaneous, and exothermic. In terms of isotherms, both the Langmuir and the Freundlich models provided reasonable fit to the experimental data, but the former was more suitable, suggesting that uptake of MB occurred on the surface by monolayer adsorption. The Dubinin-Radushkevich isotherm predicted that the sorption free energy falls between 7-8 kJ/mol and implied the physical sorption of MB by the biosorbents.

REFERENCES

1. M. F. Abou Taleb, A. Alkahtani and S. K. Mohamed, *Polym. Bull.*, **74**, 725 (2015).
2. E. Alver, A. Ü. Metin and F. Brouers, *Int. J. Biol. Macromol.*, **154**, 104 (2020).
3. A. Amedlous, O. Amadine, Y. Essamlali, H. Maati, N. Semlal and M. Zahouily, *J. Environ. Chem. Eng.*, **9**(4), 105501 (2021).
4. M. Jabli, S. G. Almalki and H. Agougui, *Int. J. Biol. Macromol.*, **156**, 1091(2020).
5. A. S. Eltaweil, I. M. Mamdouh, E. M. A. El-Monaem and G. M. El-Subruiti, *ACS Omega*, **6**(36), 23528 (2021).
6. R. Farhadi, M. A. Aroon, A. Ebrahimian Pirbazari, M. Safarpour, T. Matsuura and P. Seirafia, *Environ. Technol.*, In press (2021).
7. Z. Yang, M. Li, M. Yu, J. Huang, H. Xu, Y. Zhou, P. Rui and X. Song, *Chem. Eng. J.*, **303**, 1 (2016).
8. B. Işık and V. Uğraşkan, *Int. J. Biol. Macromol.*, **167**, 1156 (2021).
9. M. Pakizeh, F. Azinfar, M. Safarnia and F. Raji, *Sep. Sci. Technol.*, **57**(11), 1788 (2022).
10. N. Boukhalfa, M. Boutahala, N. Djebri and A. Idris, *J. Mol. Liq.*, **275**, 431 (2019).
11. N. Djebri, M. Boutahala, N. Chelali, N. Boukhalfa and L. Zeroual, *Int. J. Biol. Macromol.*, **92**, 1277 (2016).
12. Y. Li, Sh. Liu, F. Chen and J. Zuo, *J. Chem. Eng. Data*, **64**(12), 5469 (2019).
13. F. Elmi, R. Chenarian Nakhaei and H. Alinezhad, *Water Sci. Technol.*, **18**(4), 1406 (2018).
14. A. Shameem, P. Devendran, V. Siva, K. S. Venkatesh, A. Manikandan, S. Asath Bahadur and N. Nallamuthu, *J. Inorg. Organomet. Polym. Mater.*, **28**, 671 (2018).
15. A. Zahir, Z. Aslam, M. S. Kamal, W. Ahmad, A. Abbas and R. Shawabkeh, *J. Mol. Liq.*, **244**, 211 (2017).
16. A. Khawar, Z. Aslam, S. Javed and A. Abbas, *Chem. Eng. Commun.*, **205**(11), 1555 (2018).
17. A. Khawar, Z. Aslam. A. Zahir, I. Akbar and A. Abbas, *Int. J. Biol. Macromol.*, **122**, 667 (2019).
18. I. Tahira, Z. Aslam, A. Abbas, M. Monim-Ul-Mehboob, S. Ali and A. Asghar, *Int. J. Biol. Macromol.*, **136**, 1209 (2019).
19. A. Azin, A. Dadvand Koohi and B. Padekan, *Polym. Bull.*, In press (2022).
20. M. Rahmani and A. Dadvand Koohi, *Polym. Bull.*, In press (2021).
21. C. Ammar, F. M. Alminderej, Ya. EL-Ghoul, M. Jabli and Md. Shafiquzzaman, *Polym. J.*, **13**(3), 411 (2021).
22. L. Hou and P. Wu, *Carbohydr. Polym.*, **205**, 420 (2019).
23. S. Asadi, S. Eris and S. Azizian, *ACS Omega*, **3**(11), 15140 (2018).
24. M. Jabli and B. B. Hassine, *Int. J. Biol. Macromol.*, **117**, 247 (2018).
25. Y. Guesmi, H. Agougui, R. Lafi, M. Jabli and A. Hafian, *J. Mol. Liq.*, **249**, 912 (2018).
26. N. Alamin, A. Sada Khan, A. Nasrullah, J. Iqbal, Z. Ullah, I. Ud Din, N. Muhammad and Sh. Zeb Khan, *Int. J. Biol. Macromol.*, **176**, 233 (2021).
27. S. Sathiskumar, G. Sivarasan, S. Vanaraj, D. Sabarinathan, S. Arulmani, P. Vinoth Kumar and K. Preethi, *Int. J. Appl. Ceram. Technol.*, **18**(3), 902 (2021).
28. H. Agougui, N. Sebeia, M. Jabli, Y. El-Ghoul and K. Boughzala, *Inorg. Chem. Commun.*, **133**, 108986 (2021).
29. D. C. Manatunga, R. M. de Silva, K. M. Nalin de Silva, N. de Silva, Sh. Bhandari, Y. Khin Yap and N. Pabakara Costha, *Eur. J. Pharm. Biopharm.*, **117**, 29 (2017).
30. M. Ferria, S. Campisia, M. Scavinia, C. Evangelistib, P. Carnitia and A. Gervasini, *Appl. Surf. Sci.*, **475**, 397 (2019).
31. P. Panneerselvam, N. Morad and K. A. Tan, *J. Hazard. Mater.*, **186**(1), 160 (2011).
32. F. Rajia, M. Pakizeh, A. Saraeian and M. Raji, *Desalin. Water Treat.*, **57**(40), 18694 (2016).
33. J. Zhang, Q. Wang and A. Wang, *Acta Biomater.*, **6**(2), 445 (2010).
34. H. Gheisari, E. Karamian and M. Abdellahi, *Ceram. Int.*, **41**(4), 5967 (2015).
35. O. V. Ovchinnikov, A. V. Evtukhova, T. S. Kondratenko, M. S. Smirnov, V. Y. Khokhlov and O. V. Erina, *Vib. Spectrosc.*, **86**, 181 (2016).
36. A. Konwar, A. Gogoia and D. Chowdhury, *RSC Adv.*, **5**, 81573 (2015).
37. O. Duman, S. Tunç, T. G. Polat and B. Kanci, *Carbohydr. Polym.*, **147**, 79 (2016).
38. A. Metin, D. Doğan and M. Can, *Mater. Chem. Phys.*, **256**, 123659 (2020).
39. E. Makhado, S. Pandey and J. Ramontja, *Int. J. Biol. Macromol.*, **119**, 255 (2018).
40. M. Ghorbani, Se. M. Nowee, Na. Ramezanian and F. Raji, *Hydrometallurgy*, **161**, 117 (2016).
41. H. Turasan, J. Bonilla, F. Bozkurt, L. Maldonado, X. Li, T. Yilmaz, R. Sadeghi and J. Kokini, *J. Food Process Eng.*, **43**(5), e13413 (2020).
42. T. Lu, T. Xiang, X. Huan and Ch. Zhao, *Carbohydr. Polym.*, **133**, 587 (2015).
43. F. Shakib, A. Dadvand Koohi and A. Kamran Pirzaman, *Water Sci. Technol.*, **75**(8), 1932 (2017).
44. F. Raji and M. Pakizeh, *Appl. Surf. Sci.*, **282**, 415 (2013).
45. K. R. Hall, L. C. Eagleton, A. Acrivos and T. Vermeulen, *Ind. Eng. Chem. Fundam.*, **5**(2), 212 (1966).
46. Y. Li, Q. Du, T. Liu, J. Sun, Y. Wang, Sh. Wu, Z. Wang, Y. Xia and L. Xia, *Carbohydr. Polym.*, **95**(1), 501 (2013).
47. L. Liu, Y. Wan, Y. Xie, R. Zhai, B. Zhang and J. Liu, *Chem. Eng. J.*, **187**, 210 (2012).
48. A. Nasrullah, A. H. Bhat, A. Naeem, M. Hasnain Isa and M. Danish, *Int. J. Biol. Macromol.*, **107**, 1792 (2018).
49. F. Raji and M. Pakizeh, *Appl. Surf. Sci.*, **301**, 568 (2014).
50. F. Raji, A. Saraeian, M. Pakizeh and F. Attarzadeh, *RSC Adv.*, **5**(46), 37066 (2015).